

Rational surface modification of Mn_3O_4 nanoparticles to induce multiple photoluminescence and room temperature ferromagnetism†

Cite this: *J. Mater. Chem. C*, 2013, **1**, 1885

Anupam Giri,^a Nirmal Goswami,^a Monalisa Pal,^a Myo Tay Zar Myint,^b Salim Al-Harhi,^c Achintya Singha,^d Barnali Ghosh,^a Joydeep Dutta^b and Samir Kumar Pal^{*a}

Surface modification can have a significant influence on the materials behavior at the nanoscale and can lead to nanostructures with novel properties. Here, we demonstrate the surface modification induced multiple photoluminescence and room temperature ferromagnetic activation of Mn_3O_4 nanoparticles (NPs). Employing a systematic variation of the ligands, their functional groups and the structural position of the functional groups, we have identified the necessary and sufficient structural requirements of the surface co-ordinating ligands, in order to induce unprecedented optical/magnetic responses from the NPs. Using a multitude of spectroscopic techniques, we have investigated the mechanism behind the emergence of the multiple photoluminescence (PL), and it is revealed that the presence of a α -hydroxy carboxylate moiety in the ligands is necessary to activate the Jahn–Teller (J–T) splitting of Mn^{3+} ions on the NP surface and the corresponding d–d transitions along with the ligand-to-metal charge transfer transitions (LMCT, associated with $\text{Mn}^{2+/3+}$ –ligand interactions) is the key factor. However, the presence of a carboxylate group on the surface coordinating ligands is sufficient to activate the room temperature ferromagnetism of the NPs. Moreover, it has been observed that the ligands that induced the smallest crystal field splitting energy (CFSE) resulted in the strongest ferromagnetic activation of the NPs. Finally, the functionalized material has been identified as an efficient catalyst for the photo-degradation of a model cationic organic dye. Apart from the fundamental scientific interest, these results represent a promising route for the rational design of Mn_3O_4 NPs adaptable to diverse applications.

Received 25th November 2012
Accepted 8th January 2013

DOI: 10.1039/c3tc00709j

www.rsc.org/MaterialsC

Introduction

Over the past decade, magnetic nanoparticles (NPs) of the 3d transition metal oxides have attracted enormous interest due to their potential applications in various fields ranging from catalysis,¹ energy storage² and magnetic data storage³ to drug delivery and biomedical imaging.⁴ In particular, colloidal metal-oxide materials fabricated on a nanoscale can exhibit better optical, magnetic, thermal and electrical properties than the

corresponding bulk materials.⁵ Therefore, long-term endeavors have been focused on the morphology controllable synthesis and functionalization of nanocrystals for their advanced physicochemical properties and technological applications.⁶

As an important functional metal oxide, manganese oxides have attracted considerable attention because of their potential applications in diverse areas, including catalysis,⁷ rechargeable lithium ion batteries,⁸ molecular adsorption, gas sensing and in magnetics.⁹ Among them, Mn_3O_4 has been demonstrated to be one of the most inexpensive and earth-abundant catalysts and has exhibited excellent bifunctional oxygen electrode activity¹⁰ (similar to those of best known precious metal catalysts: platinum, ruthenium, and iridium), as well as being an active catalyst for the oxidation of methane and carbon monoxide.¹¹ Most recently, hollow Mn_3O_4 NPs have been utilized as positive MRI contrast agents (exploiting their room temperature paramagnetism) with an enhanced relaxivity attributed to an increased water-accessible surface area and the flexibility of further functional surface modifications.¹² However, despite the recent advances, to date, studies of any synthesis/surface modification techniques for achieving Mn_3O_4 NPs having intrinsic photoluminescence and/or room temperature

^aUnit for Nano Science & Technology, S. N. Bose National Centre for Basic Sciences, Block JD, Sector III, Salt Lake, Kolkata 700 098, India. E-mail: skpal@bose.res.in

^bChair in Nanotechnology, Water Research Center Sultan Qaboos University, Al-Khouth, Sultanate of Oman

^cPhysics Department, Sultan Qaboos University, Al-Khouth, Sultanate of Oman

^dDepartment of Physics, Bose Institute, 93/1, Acharya Prafulla Chandra Road, Kolkata 700 009, India

† Electronic supplementary information (ESI) available: (A) UV-vis absorption spectrum of as-prepared Mn_3O_4 NPs; (B) UV-vis absorption spectrum of diluted solution of lactate- Mn_3O_4 NPs; (C) the EDX spectrum of T- Mn_3O_4 NPs; (D) fluorescence microscopic images of powder as-prepared Mn_3O_4 NPs; (E) PL spectra of succinate- Mn_3O_4 NPs; (F) XRD pattern of as-prepared Mn_3O_4 NPs; G. XPS survey spectrum of T- Mn_3O_4 NPs. See DOI: 10.1039/c3tc00709j

ferromagnetism are sparse in the existing literature. In particular, the effects of capping ligands, especially how they regulate the surface properties of Mn_3O_4 NPs and the subsequent appearance of novel optical/magnetic properties, have not been studied thoroughly. Besides being of fundamental scientific interest, such an understanding is important for optimizing nanoparticle properties. So, it would be of great interest to develop approaches to control the surface chemistry to gain a better understanding the origin of surface-induced optical and magnetic properties, as subtle differences in ligand functional groups or the structural position of the functional groups can dramatically change the optical/magnetic responses.

In this report, we have used a procedure published by Lei *et al.*¹³ to synthesize Mn_3O_4 NPs and carried out a series of surface modification studies by systematic variation of the nature of the surface-protecting ligands. We define how these NP–ligand interactions modify the electronic properties of the NPs that ultimately govern multiple PL starting from blue, cyan and green to near IR under mild conditions. Most importantly, by a logical variation of the functional groups and their structural positions, we have identified the necessary and sufficient structural requirements of the ligands, to induce such novel optical/magnetic responses from the NPs upon functionalization. Although, all the ligands used in our study offer ligand-to-metal charge transfer transitions (LMCT), the presence of an α -hydroxy carboxylate moiety in the capping ligand appears to be necessary to activate the Jahn–Teller (J–T) splitting of Mn^{3+} ions in the NPs which corresponds to the d–d transitions and is the deciding factor in inducing the optical responses. Among all the ligands, we have studied tartrate (having two α -hydroxy carboxylate moieties) functionalized Mn_3O_4 NPs (will be referred as T- Mn_3O_4 NPs henceforth) in detail as the optical responses induced by tartrate have been optimal. The magnetic properties of the Mn_3O_4 NPs have also been found to be strongly ligand-dependent. We have shown that the presence of a carboxylate group in the surface coordinated ligands is sufficient to activate room temperature ferromagnetism. Moreover, a relationship between the nature of the surface bound ligands and magnetic responses of the NPs upon functionalization has been demonstrated employing the crystal field splitting energy (CFSE) of the surface Mn^{3+} ions. Uses of Mn_3O_4 nanocrystals having different morphologies as a catalyst for the degradation of a cationic organic dye have been reported recently; however, in all cases the degradation rate is very slow.¹⁴ We have observed that our surface modified T- Mn_3O_4 NPs have a better photocatalytic activity towards a model cationic organic dye (methylene blue) compared to other existing reports, thus, we infer that the increased surface reactivity and PL of T- Mn_3O_4 NPs plays an important role in enhancing the catalytic activity.

Experimental section

Materials

Glycerol, ethanol amine, guanidine, succinic acid, glycine, thioglycolic acid, lactic acid, serine, tartaric acid, sodium hydroxide, manganese chloride, 2-amino-purine (2AP) and potassium bromide (KBr) were obtained from Sigma-Aldrich

(USA) and used as received without further purification. 4',6-Diamidino-2-phenylindole (DAPI), Hoechst (H33258) and ethidium bromide (EtBr) were obtained from Molecular Probes. IR-125 was obtained from Exciton.

Synthesis of bulk Mn_3O_4 NPs

We have synthesized the bulk Mn_3O_4 nanoparticles following a reported procedure where an ultrasonic-assisted approach was used to prepare colloidal Mn_3O_4 nanoparticles at normal temperature and pressure without any additional surfactants or templates.¹³ The X-ray diffraction (XRD) patterns of the as-synthesized NPs are shown in Fig. S6.† All diffraction peaks in the figure are perfectly indexed in the literature to the tetragonal structure of Mn_3O_4 (hausmannite).¹³

Functionalization of as-prepared Mn_3O_4 NPs by different ligands to prepare ligand functionalized- Mn_3O_4 NPs

In all cases, first we have prepared 0.5 M ligand solutions in Milli-Q (from Millipore) water. Then we have adjusted the pH of the solutions to ~ 7 by the addition of 1 M sodium hydroxide (NaOH) solution. In the ligand solution of pH ~ 7 , we have added as-prepared Mn_3O_4 NPs (approximately 100 mg powder Mn_3O_4 NPs in 5 mL ligand solution), followed by extensive mixing for 12 hours in a cyclo-mixer. Finally, the non-functionalized bigger NPs were filtered out (using a syringe filter of 0.22 μm diameter) and the resulting filtered solutions were used for our experiments.

Further surface modification of T- Mn_3O_4 NPs to make them highly photoluminescent

We increased the pH of the greenish-yellow T- Mn_3O_4 NP solution from pH ~ 7 to 12 by the drop wise addition of 1 M sodium hydroxide (NaOH) solution. The greenish-yellow color of the solution turns to yellowish-brown (indicating the conversion of surface Mn^{2+} to Mn^{3+} , as in acidic/neutral pH, Mn^{3+} ions are unstable and tend to disproportionate into Mn^{2+} and Mn^{4+} , whereas it is stabilized by the comproportionation of Mn^{2+} and Mn^{4+} in alkaline conditions)¹⁵ and the resulting solution was heated at 70 °C with vigorous stirring for 10–14 hours. Finally, the solution became highly photoluminescent. It should be noted that we have diluted the as prepared T- Mn_3O_4 NP solution about 2–3 times with 0.5 M tartrate solution before high pH and temperature treatment in order to avoid precipitation of the solubilized NPs.

Sample preparation for magnetic measurements

For magnetic characterization, to get a better signal, we have used ~ 2 times more as-prepared Mn_3O_4 NPs (200–250 mg in 5 mL 0.5 M ligand solutions at pH ~ 7 followed by 24 hours of mixing) during solubilization to prepared ligand functionalized NPs, followed by pH and temperature treatment. Finally, the NP solutions were dialyzed (to remove excess ligands), lyophilized and dried over a water bath to obtain the powder samples.

Characterization techniques

Optical spectra of the solutions were recorded with a Shimadzu Model UV-2450 spectrophotometer using a quartz cuvette of 1 cm path length. The characteristic fluorescence excitation and PL spectra of the ligand functionalized-Mn₃O₄ NP solutions were recorded on a Jobin Yvon Model Fluoromax-3 fluorimeter.

TEM samples were prepared by dropping sample stock solutions onto a 300-mesh carbon coated copper grid and dried overnight in air. Particle sizes were determined from micrographs recorded using a FEI TecnaiTF-20 field-emission high-resolution transmission electron microscope operating at 200 kV.

XPS measurements were carried out using an Omicron Nanotechnology instrument equipped with seven channeltrons with a binding energy resolution of 0.1 eV. XPS was performed using monochromatic Al K α X-rays (1486.6 eV). The X-ray source was at 15 keV with the emission current of the filament of 20 mA. All measurements were done under ultrahigh vacuum conditions of 5×10^{-10} mbar. Electron flooding was employed for sample charging compensation during the measurements. The binding energies were calibrated with respect to an adventitious C 1s feature at 284.6 eV and the internal oxygen peak. XPS spectra were deconvoluted to their individual components using a Gaussian Lorentzian function after background subtraction with a Shirley function using Casa XPS software.

A JASCO FTIR-6300 spectrometer was used for the Fourier transform infrared spectroscopy (FTIR) to confirm the covalent attachment of the tartrate molecules with the Mn₃O₄ NPs. For FTIR measurements, powdered samples were mixed with KBr powder and pelletized. The background correction was made by using a reference of KBr pellets.

Raman scattering measurements were performed in a back scattering geometry using a micro-Raman setup consisting of a spectrometer (model LabRAM HR, Jobin Yvon) and a Peltier-cooled charge-coupled device (CCD) detector. An air cooled argon ion laser with a wavelength of 488 nm was used as the excitation light source. Raman spectra of all the samples have been recorded at room temperature in the frequency range 50–4000 cm⁻¹.

Magnetic measurements were performed in a Lake Shore VSM with an electromagnet that can produce a field of up to 1.6 T.

XRD patterns were obtained by employing a scanning rate of 0.02° s⁻¹ in the 2 θ range from 10° to 80° by a PANalytical XPERT-PRO diffractometer equipped with Cu K α radiation (at 40 mA and 40 kV).

Fluorescence micrographs of as-prepared Mn₃O₄ and T-Mn₃O₄ NPs were taken using an Olympus BX51 fluorescence microscope employing 365 and 436 excitation wavelengths generated through WBS and WGS mirror units, respectively.

Picosecond-resolved fluorescence transients were measured by using a commercially available spectrophotometer (Life Spec-ps) from Edinburgh Instruments, UK for 375 nm excitation (80 ps instrument response function, IRF). For 293 nm excitation we have used the third harmonic laser beam of 879 nm (0.5 nJ per pulse) using a mode locked Ti-sapphire laser with an 80 MHz repetition rate (Tsunami, Spectra Physics), pumped by a

10 W Millennia (Spectra Physics) followed by a pulse-peaker (rate 8 MHz) and a third harmonic generator (Spectra Physics, model 3980). The third harmonic beam was used for excitation of the sample inside the Time-Correlated-Single-Photon-Counting (TCSPC) instrument (IRF = 50 ps) and the second harmonic beam was collected for the start pulse.

The observed fluorescence transients were fitted by using a non-linear least square fitting procedure to a function

$$X(t) = \int_0^t E(t')R(t-t')dt'$$

comprising of convolution of the IRF ($E(t)$) with a sum of exponential

$$R(t) = A + \sum_{i=1}^N B_i e^{-t/\tau_i}$$

with pre-exponential factors (B_i), characteristic lifetimes (τ_i) and a background (A). The relative concentration in a multi exponential decay was finally expressed as:

$$c_n = \frac{B_n}{\sum_{i=1}^N B_i} \times 100.$$

The quality of the curve fitting was evaluated by reduced chi-square and residual data. It has to be noted that with our time resolved instrument, we can resolve at least one fourth of the instrument response time constants after the de-convolution of the IRF.

Results and discussion

Functionalization of Mn₃O₄ NPs with small organic ligands causes significant changes to their surface electronic structures. Before intentional variation of the ligands, we have examined the UV-vis electronic absorption pattern of the as-prepared Mn₃O₄ NPs alone. However, as shown in Fig. S1,† it has no such characteristic absorption signature in the UV-vis region. The absorption spectra recorded in Fig. 1 for ligand functionalized Mn₃O₄ NPs exhibit distinct features depending upon the type of ligand functional groups used. Fig. 1a–f show the absorption spectra of functionalized Mn₃O₄ NPs where –OH (hydroxyl group of glycerol), –OH and –NH₂ (hydroxyl and amine groups of ethanol amine), –NH₂ (amine group of guanidine), –COO⁻ (carboxylate group of succinate), –COO⁻ and –NH₂ (carboxylate and amine groups of glycine), and –COO⁻ and –SH (carboxylate and thiol groups of thioglycolate) functional groups of the ligands have been chosen to functionalize the NPs. In all cases, a characteristic absorption band (marked by arrows) between 300 and 360 nm has been observed. We assume that this high energy absorption band is the result of the interaction between the ligand functional groups and the Mn²⁺/Mn³⁺ on the NP surface, therefore assigned as the LMCT band. However, with the inclusion of an –OH group at the α position with respect to –COO⁻ *i.e.* in the case of lactate-Mn₃O₄ (Fig. 1g), the UV-vis absorption spectrum displays distinctly different features at the low energy region. Even more interestingly, on shifting the

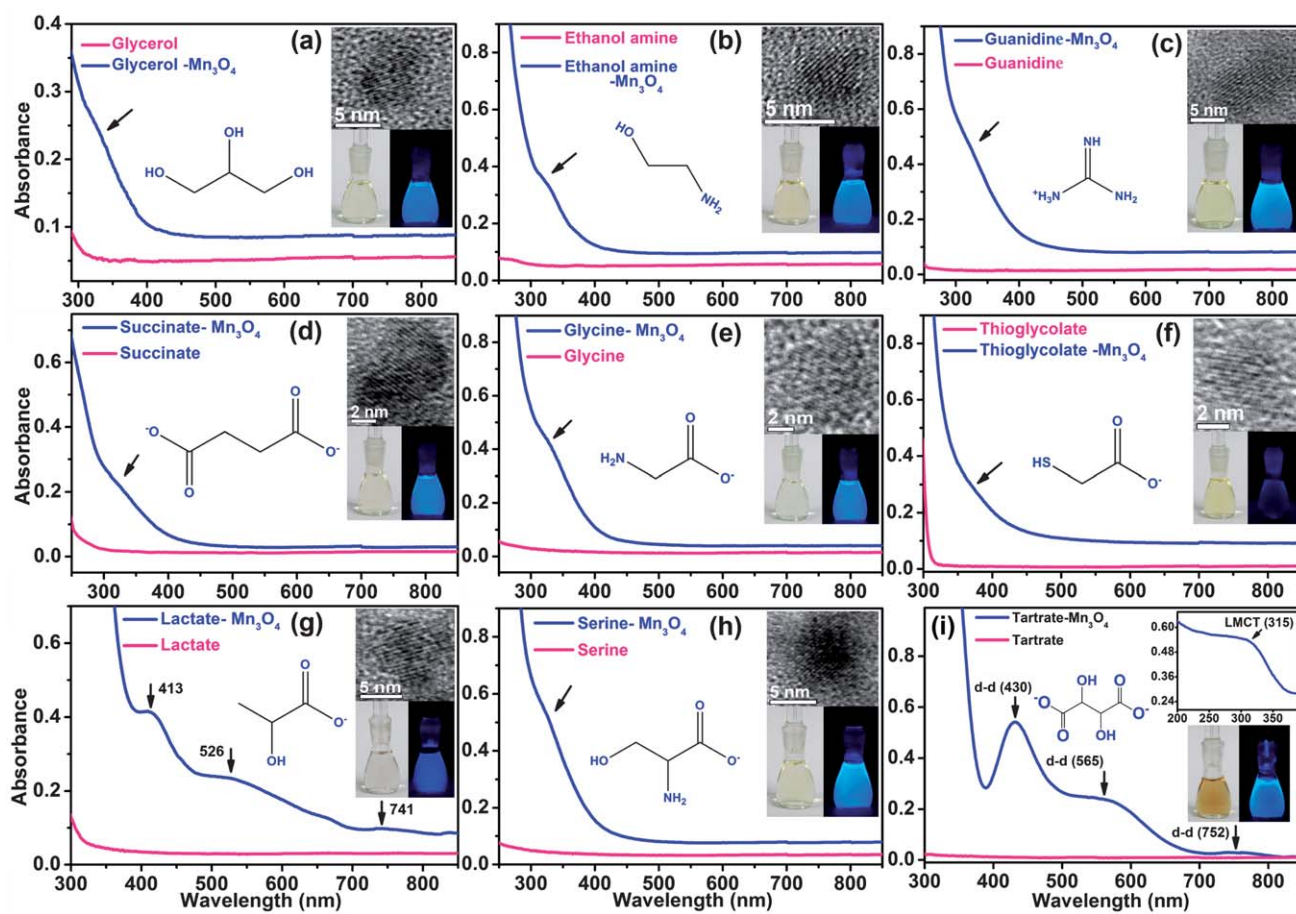


Fig. 1 (a–i) show the UV-vis absorption spectra of ligand functionalized- Mn_3O_4 NPs in aqueous solution at pH ~ 7 . Different combinations of ligand functional groups have been employed in order to activate the Jahn–Teller (J–T) splitting of Mn^{3+} ions at the NP surface and to bring out the optimal optical responses from the functionalized NPs. (a) –OH (hydroxyl) group of glycerol (b) –OH and $-\text{NH}_2$ (hydroxyl and amine) groups of ethanol amine, (c) $-\text{NH}_2$ group of guanidine, (d) $-\text{COO}^-$ (carboxylate) group of succinate, (e) $-\text{COO}^-$ and $-\text{NH}_2$ groups of glycine, (f) $-\text{COO}^-$ and $-\text{SH}$ (carboxylate and thiol) groups of thioglycolate, (g) $-\text{COO}^-$ and $-\text{OH}$ (at α position) groups of lactate, (h) $-\text{COO}^-$ and $-\text{OH}$ (at β position) groups of serine and (i) $-\text{COO}^-$ and $-\text{OH}$ (two α hydroxyl groups) groups of tartrate have been used respectively, to functionalize the as-prepared Mn_3O_4 NPs. The upper insets of (a–h) show the corresponding HRTEM images of the various ligand functionalized Mn_3O_4 NPs. Photographs of various ligand functionalized Mn_3O_4 NPs under visible (left) and UV light (right) are shown in the lower inset.

structural position of the $-\text{OH}$ group from α to β with respect to the $-\text{COO}^-$ group *i.e.* in the case of serine- Mn_3O_4 (although serine contains an α NH_2 group, however, the results of the glycine- Mn_3O_4 could be considered as a control study), those low energy UV-vis bands vanish. This observation clearly indicates that the origin of the distinct absorption features is a special case only seen for α -hydroxy carboxylate (like lactate) moiety containing ligand functionalized Mn_3O_4 NPs. To further corroborate this phenomenon, we have employed tartrate, having two α -hydroxy carboxylate groups, as a capping ligand. Akin to lactate- Mn_3O_4 , T- Mn_3O_4 possesses a LMCT band as well as distinct and even more pronounced absorption features in the low energy region. Thus, from the above investigation we can infer that the presence of an α -hydroxy carboxylate moiety in the surface coordinating ligand is necessary to activate the observed distinct absorption features (detailed identification of the absorption bands is discussed later in the text). The upper insets of Fig. 1a–h are the high resolution transmission electron microscopic (HRTEM) images of the corresponding ligand functionalized Mn_3O_4 NPs showing their tentative diameters

within 3–5 nm. The lower insets of Fig. 1a–i show the photographs of various ligand functionalized Mn_3O_4 NPs under visible (left) and UV light (right). As is evident from the photographs, except in the case of thioglycolate- Mn_3O_4 and lactate- Mn_3O_4 NPs, the other ligand functionalized NPs exhibit very bright photoluminescence under UV light. Considering the optical responses obtained from T- Mn_3O_4 NPs as optimal, we have investigated only T- Mn_3O_4 NPs in detail in order to gain an insight into the origin of these distinct absorption characteristics, bright PL under UV light and also the effect of further surface modification.

A TEM study has been carried out in order to characterize the water soluble T- Mn_3O_4 NPs in detail and also to substantiate the functionalization process. As shown in Fig. 2a, T- Mn_3O_4 NPs have a broad size distribution (1.5–5.5 nm) with an average diameter of 3.30 ± 0.14 nm (Fig. 2c) and are nearly spherical in shape. The corresponding HRTEM image (Fig. 2b) confirms the crystallinity of the NPs. The interplanar distance between the fringes is about 0.249 nm which corresponds to the distance between the (211) planes of the Mn_3O_4 tetragonal crystal lattice.

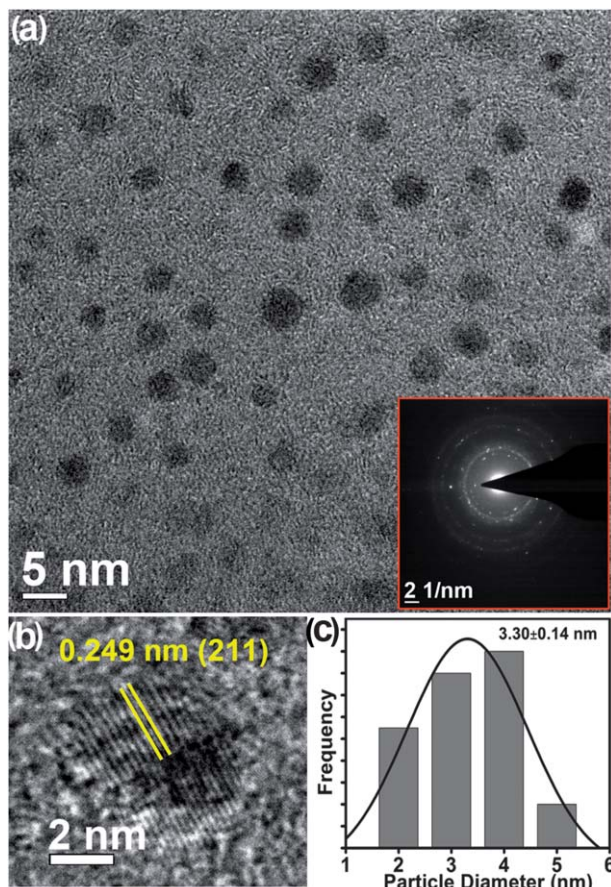


Fig. 2 (a) TEM image of T-Mn₃O₄ NPs. The inset shows the selective area electron diffraction (SAED) pattern of the T-Mn₃O₄ NPs. (b) HRTEM image of the crystalline structure of T-Mn₃O₄ NPs. (c) Size distribution of the T-Mn₃O₄ NPs.

The selective area electron diffraction (SAED) pattern (inset of Fig. 2a) also indicates the crystalline structure of the NPs. Energy dispersive X-ray (EDX) spectroscopic analysis of T-Mn₃O₄ NPs (Fig. S3†) has confirmed that the crystallites consist solely of manganese and oxygen.

In Fig. 1i, the UV-vis absorption spectra of the T-Mn₃O₄ NPs (at pH ~ 7) exhibit two absorption peaks at 315 (shown in the inset) and 430 nm, a shoulder descending into lower energies around 565 nm and a broad band at 752 nm. The observed peak at 315 nm could be assigned to the possible high energy LMCT processes involving tartrate-Mn²⁺/Mn³⁺ interactions.¹⁶ The other bands at 430, 565 and 752 nm are attributed to d-d transitions of Mn³⁺ in T-Mn₃O₄ NPs, as the degeneracy of the 5E_g ground state term of d⁴ (Mn³⁺) in a high-spin octahedral environment has been lifted by the Jahn-Teller effect, which leads to the observed bands for the transitions of 5B_{1g} → 5E_g, 5B_{1g} → 5B_{2g} and 5B_{1g} → 5A_{1g}, respectively.¹⁷ In the case of the as-prepared T-Mn₃O₄ NPs (at pH ~ 7), the LMCT excited state has been observed to be strongly photoluminescent, whereas PL from the d-d excited states has been found to be considerably weaker. Thus, in order to make the d-d excited states highly photoluminescent, we have heat-treated the as prepared T-Mn₃O₄ NPs at pH ~ 12 and 70 °C for 12 h (details in Experimental section). As can be seen from Fig. 3a, the UV-vis

absorption spectrum of the heat treated T-Mn₃O₄ NPs changes from the initial spectrum of T-Mn₃O₄ NPs (Fig. 1i). Specifically, the peak at 430 nm and the lower energy shoulder at 565 nm (both originate due to d-d transitions involving Mn³⁺) are significantly perturbed and blue shifted to 385 and 440 nm, respectively (justification later in the text). However, the LMCT band at 315 nm and another d-d band at 758 nm remain almost unaffected. The inset of Fig. 3a shows the fluorescence microscope images of powder containing T-Mn₃O₄ NPs (after treatment) under irradiation with white light (bright field, I) and light of two different wavelengths (II-365 nm and III-436 nm), respectively. Multi-color PL arising from different excitation of the NPs is clearly evident from the photographs. Fig. S4† shows the fluorescence microscope images of powder consisting of as-prepared Mn₃O₄ NPs under identical conditions, showing no such PL.

Fig. 3b shows the normalized PL spectra of T-Mn₃O₄ NPs at room temperature and pH ~ 12. Multiple PL of T-Mn₃O₄ NPs starting from blue, cyan, green to near-infrared region (PL maximum at 417, 473, 515 and 834 nm) of the spectra against excitation at four different wavelengths (315, 370, 440 and 760 nm, respectively) are clearly evident from the spectra. In the excitation spectra (Fig. 3c) of T-Mn₃O₄ NPs at their respective PL maxima, the observed peaks/bands have a direct correlation with the absorption peaks/bands involving LMCT and d-d transitions (Fig. 3a). Thus, the PL as shown in Fig. 3b may originate predominantly from the LMCT [tartrate → Mn³⁺] excited states and ligand field excited states of the metal (Mn³⁺) d orbitals. PL from either an intraligand or metal to ligand charge-transfer (MLCT) excited states are considered unlikely. In the case of other ligand functionalized Mn₃O₄ NPs having a sole LMCT absorption band, e.g. succinate-Mn₃O₄, a single PL with a maximum (λ_{max}) around 410 nm has been observed (Fig. S5†). PL quantum yields (QY) of the T-Mn₃O₄ NPs at pH ~ 12, have been calculated by using the comparative method of Williams *et al.*,¹⁸ which involves the use of well characterized standard samples with known QY values. PL QYs of 4.20% (for 417 nm PL), 2.88% (for 473 nm PL), 0.54% (for 515 nm PL) and 0.0018% (for 834 nm PL) were obtained relative to the standards 2-amino-purine (2AP), 4',6-diamidino-2-phenylindole (DAPI), Hoechst (H33258) and 2-[7-[1,3-dihydro-1,1-dimethyl-3-(4-sulfobutyl)-2H-benz[e]indol-2-ylidene]-1,3,5-heptatrienyl]-1,1-dimethyl-3-(4-sulfobutyl)-1H benz[e]indolium hydroxide, inner salt, and sodium salt (IR-125), respectively. Except for thioglycolate-Mn₃O₄ and lactate-Mn₃O₄ NPs, the PL of other ligand functionalized Mn₃O₄ NPs arises from the LMCT excited state, exhibiting QY values between 4 and 7%.

Picosecond-resolved PL decay transients of T-Mn₃O₄ NPs have been collected to further understand the origin of the PL due to the functionalization of the NPs. Fig. 3d represents the PL decay transients of T-Mn₃O₄ NPs at three different PL maxima of 410, 470 and 515 nm using three different excitation sources of 293, 375 and 445 nm wavelengths, respectively. The observed differences in the excited-state lifetime of T-Mn₃O₄ NPs at 410 nm compared to the lifetimes at 470 and 515 nm PL, suggest a difference in the origin of the PL. The average lifetime (τ) for 470 and 515 nm PL (upon excitation by 375 and 445 nm sources,

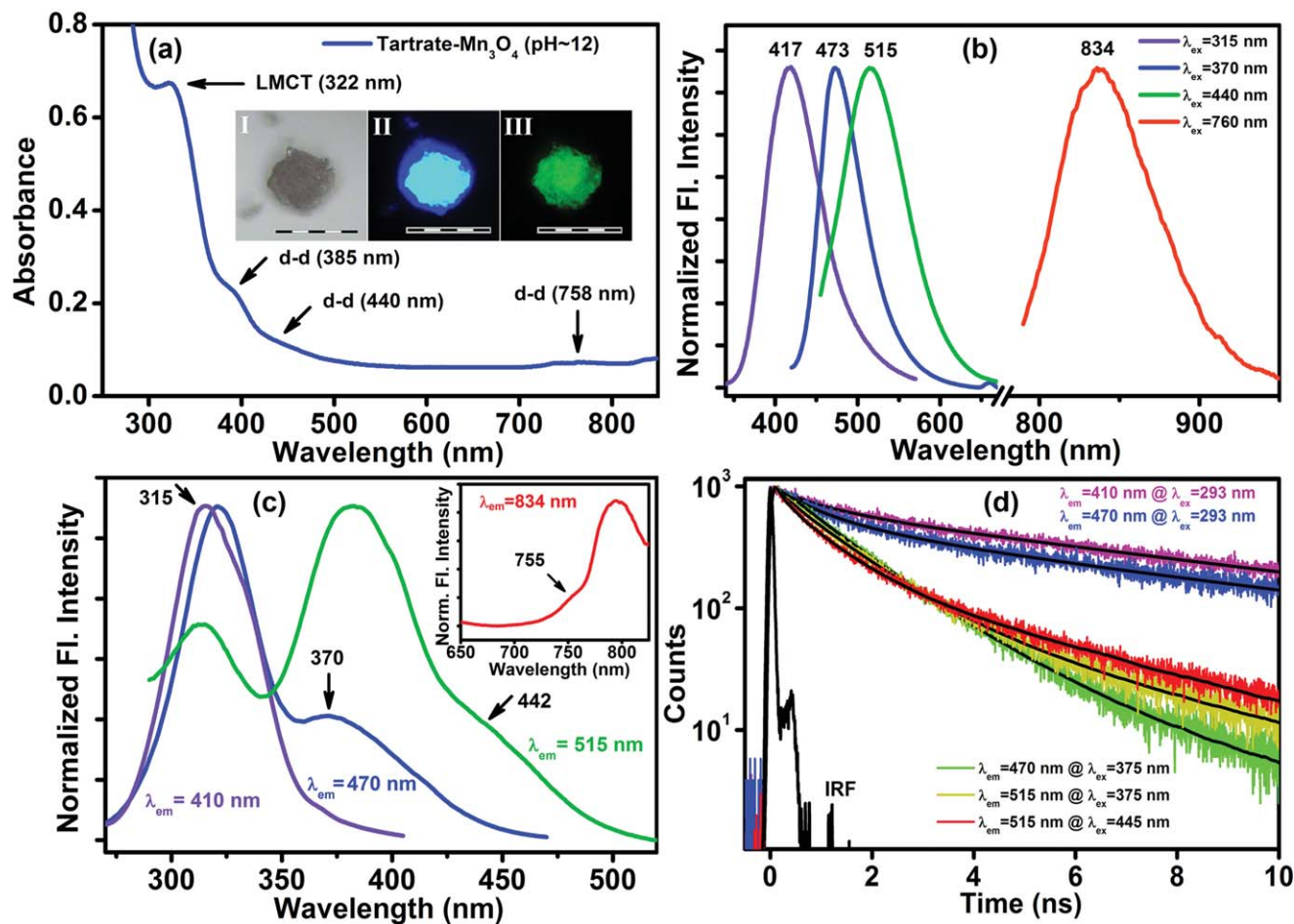


Fig. 3 (a) UV-vis absorption spectrum of T-Mn₃O₄ NPs after treatment (at pH ~ 12 and 70 °C for 12 h). The inset shows the fluorescence microscopic images of the same NPs under irradiation with white light (bright field, I) and light of two different wavelengths; 365 (II) and 436 (III) nm. The scale bars in the images are 500 μm. (b) Normalized steady-state PL spectra collected from T-Mn₃O₄ NPs at four different excitation wavelengths of 315, 370, 440 and 760 nm at pH ~ 12. (c) Excitation spectra of T-Mn₃O₄ NPs at different PL maxima of 410, 470, 515 and 834 nm. (d) Picosecond-resolved PL transients of T-Mn₃O₄ NPs in water measured at emission wavelengths of 410, 470 and 515 nm upon excitation with excitation sources of 293, 375 and 445 nm wavelengths.

respectively) have been observed to be 1.13 and 0.78 ns respectively, whereas a relatively longer τ of 5.32 ns has been observed for 410 nm PL (Table 1). Moreover, distinctly different lifetime values of 470 nm PL upon excitation using 293 (4.04 ns) and 375 (1.13 ns) nm sources clearly differentiate the origin of the two excitations. Thus, the lifetime data and steady-state measurements clearly suggest that the LMCT excited states are responsible for the PL at 417 nm, whereas the Jahn–Teller excited states lead to the PL maxima at 470, 515 and 834 nm.

In order to get supporting evidence regarding the origin of the optical properties of the T-Mn₃O₄ NPs, XPS analysis has been carried out on Mn₃O₄ NPs, before and after functionalization with sodium tartrate (Fig. 4a, traces A and B respectively). In the high-resolution spectra of Mn 2p of Mn₃O₄ (trace A), the 2p_{3/2}–2p_{1/2} doublet has been observed to be at 637.61 and 649.31 eV respectively, with a spin-orbit splitting (difference between the binding energy values of the Mn 2p_{3/2} and Mn 2p_{1/2} levels) value of 11.70 eV, which is in good agreement with

Table 1 Lifetime values of picosecond time-resolved PL transients of T-Mn₃O₄ NPs, detected at various PL maxima upon excitation at different wavelengths. The values in parentheses represent the relative weight percentages of the time components

System	λ_{ex} (nm)	PL peak, λ_{em} (nm)	τ_1 (ns)	τ_2 (ns)	τ_3 (ns)	τ_{av} (ns)
T-Mn ₃ O ₄ NPs	293	410	0.26 (11)	1.05 (29)	8.37 (60)	5.32
	293	470	0.54 (29)	1.43 (29)	8.20 (42)	4.04
	375	470	0.43 (20)	1.16 (74)	3.09 (6)	1.13
	375	515	0.18 (30)	1.06 (62)	3.93 (8)	1.03
	445	515	0.18 (47)	0.87 (44)	3.58 (9)	0.78

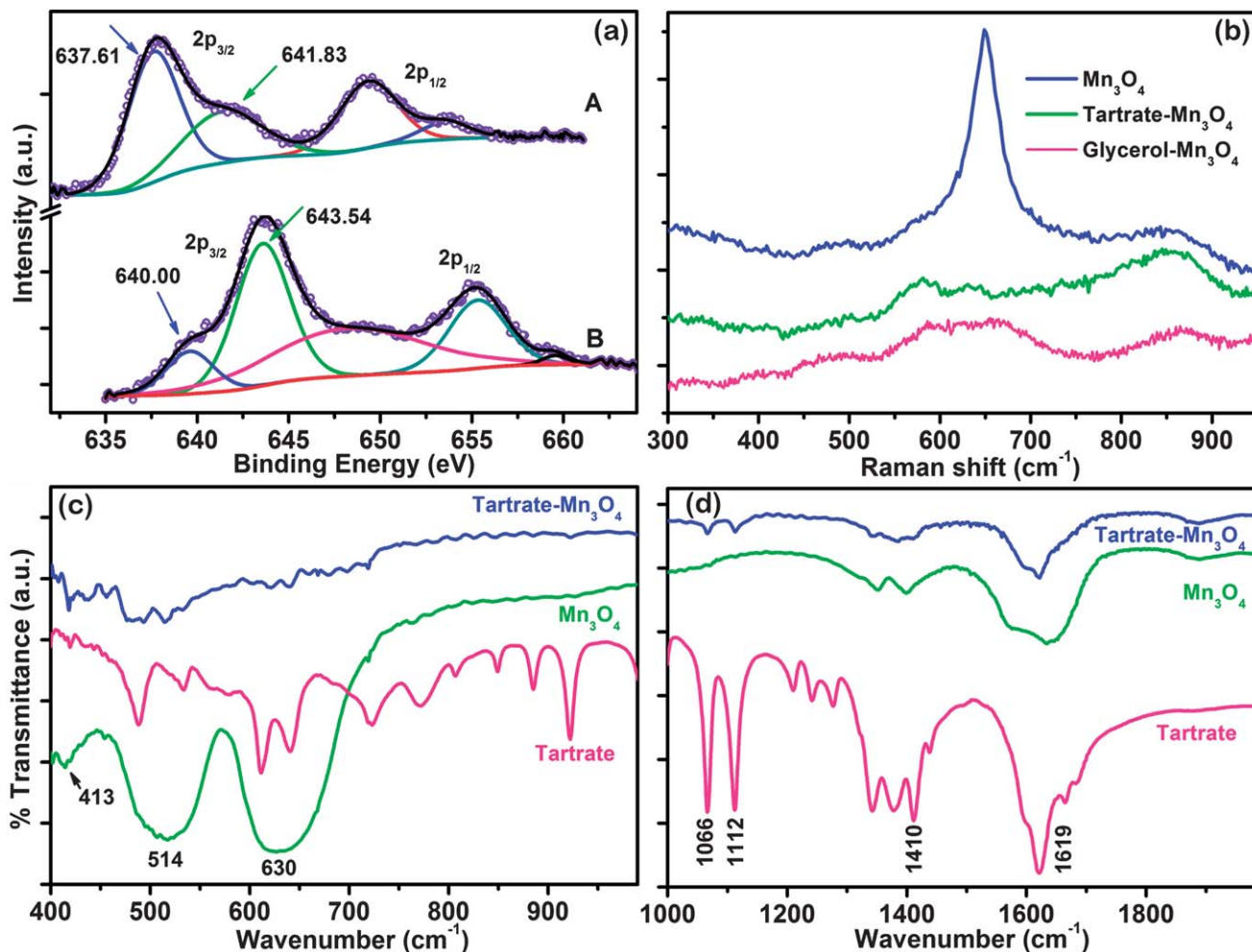


Fig. 4 (a) XPS spectra of the Mn 2p region for Mn₃O₄ NPs (trace A) and T-Mn₃O₄ NPs (trace B). (b) Raman spectra of the as prepared Mn₃O₄, glycerol-Mn₃O₄ and T-Mn₃O₄ NPs. (c and d) FTIR spectra of sodium tartrate, T-Mn₃O₄ and the as prepared Mn₃O₄ NPs recorded with a KBr pellet.

previous reports.¹⁹ The Mn 2p_{3/2} features at 637.61 and 641.383 eV are attributed to the oxides of Mn²⁺ and Mn³⁺ respectively.²⁰ In the case of T-Mn₃O₄ NPs (trace B), similar spin-orbit splitting (11.69 eV) has been observed and in the deconvoluted Mn 2p_{3/2} spectrum the peak at a binding energy of 640.00 eV is attributed to the +3 oxidation state of Mn, assuming the peak at 643.54 eV to be a shake up satellite. Greater intensity of the shake-up satellite peak could be due to the convolution of the shake-up satellite plus the shoulder just in front of the 2p_{1/2} peak. So, the presence of Mn³⁺ in the T-Mn₃O₄ NPs further supports our arguments regarding the origin of the optical properties.

Raman spectroscopy, which is a sensitive probe to the local atomic arrangements and vibrations, has been used to investigate any structural perturbations of Mn₃O₄ NPs upon their functionalization with tartrate. As is evident from Fig. 4b, we have observed a substantial perturbation of the main characteristic Raman peak (at 650 cm⁻¹, represents the Mn–O breathing vibration of divalent manganese ions in tetrahedral coordination²¹) of Mn₃O₄ NPs²² as a result of tartrate functionalization. Thus, the drastic perturbation of the symmetric stretching of the tetragonal Mn₃O₄ structure (corresponding to

650 cm⁻¹ peak²³) provides a strong physical basis for the origin of the novel optical properties of the NPs upon functionalization. A similar perturbation of the 650 cm⁻¹ peak in the case of glycerol-Mn₃O₄ NPs further indicates that the decrease of the Raman peak does not originate from Jahn–Teller splitting, rather it is the outcome of ligand functionalization.

To obtain direct evidence of the covalent functionalization of Mn₃O₄ NPs with tartrate ligands, FTIR measurements have been performed on both as-prepared and tartrate functionalized Mn₃O₄ NPs along with tartrate itself. As shown in Fig. 4c, bare as-prepared Mn₃O₄ NPs exhibit three characteristic bands (in the range of 400–1000 cm⁻¹) at 630, 514 and 413 cm⁻¹, which are associated with the stretching vibrations of Mn–O and Mn–O–Mn bonds.²⁴ However, these bands are not distinctly visible after functionalization (*i.e.* in the case of the T-Mn₃O₄ NPs), suggesting a potent surface modification of the NPs has taken place upon interaction with tartrate ligands. On the other hand, in the case of tartrate, the appearance of two sharp bands at 1066 and 1112 cm⁻¹ could be reasonably assigned to the C–OH stretching modes of tartrate.²⁵ However, substantial broadening of these two bands upon attachment to the NP

surface strongly indicates their significant interaction with the surface of the NPs. Moreover, considerable perturbation of the symmetric (1410 cm^{-1}) and asymmetric (1619 cm^{-1}) stretching modes of the carboxylate groups (COO^-) of tartrate²⁶ in T- Mn_3O_4 NPs clearly confirms the covalent binding of carboxylate's oxygen with the NP surface.

To study the effect of the surface bound ligands on the magnetic behaviour of Mn_3O_4 NPs, we have characterized both the as-prepared and ligand functionalized NPs, where the nature of the surface ligands was varied depending on their functional groups. Fig. 5 shows the applied field dependent magnetization measurements (M - H curves) at room temperature (300 K). The M - H curve (inset of Fig. 5a) of as-prepared Mn_3O_4 NPs is linear with the applied field and has no hysteresis loop at 300 K, indicating the paramagnetic behaviour of the nanocrystals, which is as expected. However, at 300 K, the M - H curves of each of the ligand functionalized- Mn_3O_4 NPs demonstrate a distinctly different magnetization response compared to the as-prepared NPs. Clearly, each ligand evokes a different magnitude of ferromagnetism to the as-prepared Mn_3O_4 NPs upon functionalization. While the room temperature ferromagnetism can be activated by functionalization with glycerol and guanidine, it can be further enhanced by succinate

and tartrate (Fig. 5a-d). Both succinate and tartrate functionalized Mn_3O_4 NPs show well-defined hysteresis loops with saturation magnetization and coercive fields (H_C) of around $2 \times 10^{-3}\text{ emu g}^{-1}$ and 105 Oe, respectively. Several investigations showed that this kind of room temperature ferromagnetism could be controlled by surface treatments of the nanocrystals, although, most of these studies have been focused mainly on transition metal doped ZnO and TiO_2 nanomaterial systems.²⁷ Unfortunately, the exact origin of such room temperature ferromagnetic activation of Mn_3O_4 nanocrystals is not known at the present time. However, based on the correlation between the crystal field splitting energy (CFSE) of Mn^{3+} ions upon interaction with the ligand fields and the increase in coercive force from glycerol- Mn_3O_4 to succinate- Mn_3O_4 NPs, one might expect that the field strength of the functional ligands is at play. According to ligand field theory, transition metal ions having a larger d orbital splitting energy due to ligand coordination should have a smaller spin-orbit coupling.²⁸ Any decrease in the spin-orbit coupling of surface magnetic cations results in a smaller surface magnetic anisotropy and subsequently the coercivity of the NPs will be reduced.²⁹ It is also well known that σ donor ligands result in larger CFSEs than π donors.²⁸ Among the four ligands used for the magnetic measurements, glycerol

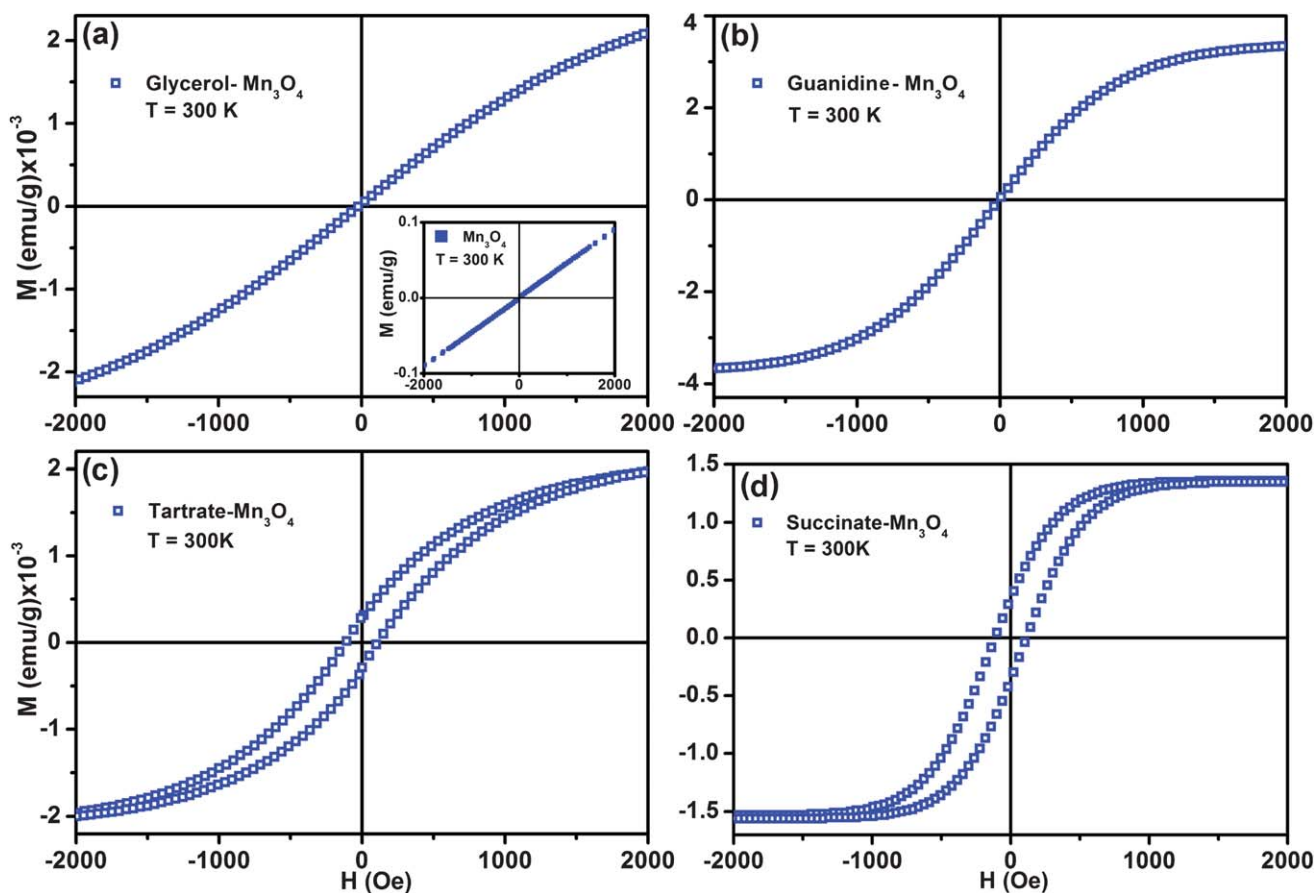


Fig. 5 Field dependent magnetization (M vs. H) at room temperature (300 K) (a) glycerol- Mn_3O_4 , (b) guanidine- Mn_3O_4 , (c) tartrate- Mn_3O_4 and (d) succinate- Mn_3O_4 NPs. The inset shows the same for as-prepared Mn_3O_4 NPs. The distinct hysteresis loops observed in the cases of (c) and (d) confirm ferromagnetic activation of the NPs upon functionalization with carboxylate ligands.

(having an –OH group) and guanidine (–NH₂) are σ donors, with tartrate having both σ donor (–OH) and π donor (–COO[–]) properties, whereas, succinate (having only –COO[–]) is a π donor ligand.²⁸ Thus, because of the higher CFSEs, glycerol and guanidine functionalized Mn₃O₄ NPs show no coercivity, however, tartrate and succinate functionalized NPs show coercivity of 97.5 and 109 Oe, respectively. Very recently, Zhang *et al.* also described similar regulation of magnetic behavior in the case of surface modified (using sodium bis[2-ethylhexyl]sulfosuccinate, AOT) Mn-doped ZnO nanorods, on the basis of ligand field multiplet theory and the ligand-to-metal charge transfer effects.³⁰ Their theoretical simulation results indicate that both different surface modification induced alteration of the Mn³⁺ (3d⁴)-ligand anion p-orbital hybridization strength and the density of a midgap state with strong O 2p character have been correlated to the observed ferromagnetism. Since the XPS study confirms the presence of Mn³⁺ ions at the surface of the functionalized NPs and the FTIR study substantiates the strong interactions of carboxylate and hydroxyl groups with the nanoparticle surface (in the case of T-Mn₃O₄ NPs), we anticipate that surface modification induced alteration of the Mn³⁺ (3d⁴)-ligand anion p orbital hybridization strength can also play a crucial role in the observed ferromagnetic activation of succinate and tartrate functionalized Mn₃O₄ NPs. This observation of room temperature ferromagnetism is an important enabling result and encouraging from a fundamental perspective.

Finally, considering the growing interest of manganese oxide based nanostructures as catalysts,^{14a} the photocatalytic activity of magneto-luminescent T-Mn₃O₄ NPs has been evaluated by measuring the decomposition rates of methylene blue (MB) under irradiation with UV light. MB is a common cationic dye used in the textile industry and is also known to be an excellent probe for the study of interfacial electron transfer in colloidal semiconductor systems.³¹ To measure the UV light-induced chemical processes with spectroscopic precision, we have used a versatile fiber-optic based system for sensitive optical measurements in strong ambient light.³² The characteristic absorption of MB at 660 nm has been chosen for monitoring the photocatalytic process with T-Mn₃O₄ NPs under UV light at room temperature. We have recorded the absorption spectra of MB at 30 second intervals, using SPECTRA SUITE software supplied by Ocean Optics, and finally plotted the MB absorption at 660 nm against the time of photo-irradiation. Fig. 6 shows the relative concentration (C_t/C_0) of MB (in the absence and presence of T-Mn₃O₄ NPs) in solution plotted against the UV irradiation time. The photodegradation curve of MB in the presence of T-Mn₃O₄ NPs has been found to follow a first-order exponential equation with a kinetic rate constant (k) of $5.23 \times 10^{-2} \text{ s}^{-1}$ and a total photodegradation of 48% within 40 minutes of irradiation. In photocatalytic reactions, the major energy wasting step is the recombination of photo-generated electrons and holes, leading to a low quantum yield for the process. However, this recombination process is reduced as the particle size goes down and consequently better transfer of the photogenerated electrons and holes to the surface bound molecules increases the efficiency of photocatalysis.³³ Moreover, this electron-hole recombination could be prevented by adding

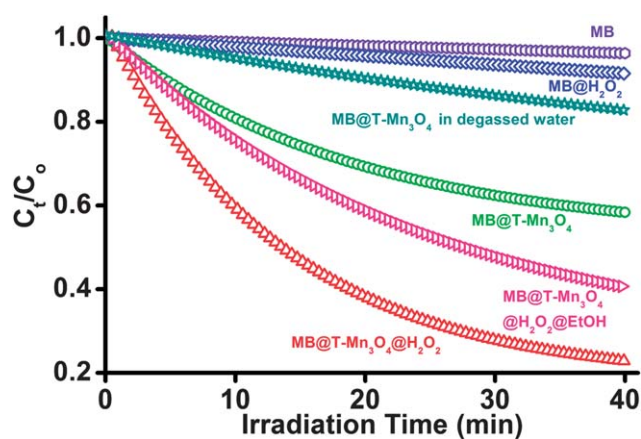


Fig. 6 Plots of relative concentration (C_t/C_0) versus time for the photodegradation of MB (monitored at 660 nm) alone and in the presence of T-Mn₃O₄ NPs, H₂O₂, T-Mn₃O₄@H₂O₂ and T-Mn₃O₄@H₂O₂@EtOH, are shown.

a proper electron acceptor such as H₂O₂ in to the system. Acting as an electron acceptor and also as a source of $\cdot\text{OH}$ radical, H₂O₂ increases the photocatalytic activity in both ways. We do observe this postulated fact by the addition of a small amount of H₂O₂ (final concentration of 415 μM) into the MB@T-Mn₃O₄ reaction mixture. As observed from Fig. 6, upon addition of H₂O₂ the photodegradation of MB was enhanced significantly (with a kinetic rate constant (k) of $7.25 \times 10^{-2} \text{ s}^{-1}$ and total photodegradation of 85% for the same 40 minute period of irradiation). In order to confirm the involvement of $\cdot\text{OH}$ radicals in the photocatalytic process, we have examined the effect of an $\cdot\text{OH}$ scavenging agent (ethanol) and oxygen free environment (achieved by 2 hours of argon flow into the reaction mixture before UV irradiation) on the degradation process. As shown in Fig. 6, in both cases, a reduction of the photocatalytic rate was observed, which validates the role of $\cdot\text{OH}$ radicals in the photocatalytic process. Zhan and co-workers have recently demonstrated the degradation of methylene blue using Mn₃O₄ nanocrystals at 80 °C and in the presence of H₂O₂, however, in the absence of H₂O₂ no obvious MB degradation was observed for up to 3 h.^{14b} Thus, we infer that the small average diameter, favorable surface functionalization (by tartrate) for cationic MB attachment and most importantly the photoluminescence of T-Mn₃O₄ NPs, plays the beneficial role to accelerate the photocatalytic activity of Mn₃O₄ NPs.

Conclusions

Surface modification of Mn₃O₄ NPs with a series of small organic ligands provides a good platform for studying the effects of surface chemistry on the optical/magnetic responses of the NPs. In all cases, LMCT optical bands in the electronic spectra are present and are found to be almost independent of the nature of the ligands. However, among the wide variety of ligands, only α -hydroxy carboxylate containing ligands can activate the Jahn–Teller (J–T) splitting of Mn³⁺ ions. Apparently, the optical response of NPs to the surface modification enables the elucidation of the quantum origins of multiple PL

properties, which are further corroborated by time resolved lifetime studies. Convergent evidence from XPS, FTIR and Raman analyses shows that the coordinating-capping ligand can greatly affect the surface of Mn_3O_4 NPs. Moreover, the presence of a carboxylate group in the surface coordinating ligands is found to be sufficient to activate the room temperature ferromagnetism of the NPs. A correlation between the nature of the surface bound ligands and the magnetic responses of the functionalized NPs has been demonstrated employing crystal field splitting energy (CFSE) of the Mn^{3+} ions. Finally, we have evaluated the photocatalytic activity of T- Mn_3O_4 NPs by monitoring the degradation of an organic pollutant under UV irradiation and an enhanced photocatalytic activity of the NPs has been observed. We believe that this work represents a step forward in the rational design of multifunctional NPs and the approach developed to systematically alter the NP surface chemistry could also be applied more generally to the investigation of other manganese oxides and various manganese doped NPs.

Acknowledgements

A.G. thanks UGC, India, for fellowship. N.G. thanks CSIR, India, for fellowship. We thank DST for financial grant DST/TM/SERI/2k11/103. Authors would like to thank Sultan Qaboos University for providing the XPS facility used in this study. We thank Mr Samik Roy Moulik and Mr Dipankar Roy for performing TEM and VSM measurements of the functionalized Mn_3O_4 NPs, respectively.

Notes and references

- (a) T. Zeng, W.-W. Chen, C. M. Cirtiu, A. Moores, G. Song and C.-J. Li, *Green Chem.*, 2010, **12**, 570–573; (b) R. Hudson, A. Riviere, C. M. Cirtiu, K. L. Luska and A. Moores, *Chem. Commun.*, 2012, **48**, 3360–3362.
- P. Simon and Y. Gogotsi, *Nat. Mater.*, 2008, **7**, 845–854.
- T. Hyeon, *Chem. Commun.*, 2003, 927–934.
- (a) N. Lee and T. Hyeon, *Chem. Soc. Rev.*, 2012, **41**, 2575–2589; (b) Q. A. Pankhurst, N. T. K. Thanh, S. K. Jones and J. Dobson, *J. Phys. D: Appl. Phys.*, 2009, **42**, 224001–224016; (c) R. Mout, D. F. Moyano, S. Rana and V. M. Rotello, *Chem. Soc. Rev.*, 2012, **41**, 2539–2544.
- (a) M. A. El-Sayed, *Acc. Chem. Res.*, 2001, **34**, 257–264; (b) R. Narayanan and M. A. El-Sayed, *J. Phys. Chem. B*, 2005, **109**, 12663–12676; (c) S. Laurent, D. Forge, M. Port, A. Roch, C. Robic, L. Vander Elst and R. N. Muller, *Chem. Rev.*, 2008, **108**, 2064–2110; (d) M. B. Cortie and A. M. McDonagh, *Chem. Rev.*, 2011, **111**, 3713–3735.
- (a) E. Oh, K. Susumu, R. Goswami and H. Mattoussi, *Langmuir*, 2010, **26**, 7604–7613; (b) Y. Peng, A.-W. Xu, B. Deng, M. Antonietti and H. Cölfen, *J. Phys. Chem. B*, 2006, **110**, 2988–2993; (c) X. H. Huang, Z. Y. Zhan, X. Wang, Z. Zhang, G. Z. Xing, D. L. Guo, D. P. Leusink, L. X. Zheng and T. Wu, *Appl. Phys. Lett.*, 2010, **97**, 203112; (d) A. Giri, N. Goswami, M. S. Bootharaju, P. L. Xavier, R. John, N. T. K. Thanh, T. Pradeep, B. Ghosh, A. K. Raychaudhuri and S. K. Pal, *J. Phys. Chem. C*, 2012, **116**, 25623–25629; (e) N. Goswami, A. Giri, S. Kar, M. S. Bootharaju, R. John, P. L. Xavier, T. Pradeep and S. K. Pal, *Small*, 2012, **8**, 3175–3184; (f) A. Giri, A. Makhil, B. Ghosh, A. K. Raychaudhuri and S. K. Pal, *Nanoscale*, 2010, **2**, 2704–2709.
- T. Yamashita and A. Vannice, *Appl. Catal., B*, 1997, **13**, 141–155.
- (a) M. M. Thackeray, *Prog. Solid State Chem.*, 1997, **25**, 1–71; (b) D. K. Kim, P. Muralidharan, H.-W. Lee, R. Ruffo, Y. Yang, C. K. Chan, H. Peng, R. A. Huggins and Y. Cui, *Nano Lett.*, 2008, **8**, 3948–3952.
- (a) W. S. Seo, H. H. Jo, K. Lee, B. Kim, S. J. Oh and J. T. Park, *Angew. Chem., Int. Ed.*, 2004, **43**, 1115–1117; (b) Y. F. Shen, R. P. Zerger, R. N. DeGuzman, S. L. Suib, L. McCurdy, D. I. Potter and C. L. O'Young, *Science*, 1993, **260**, 511–515.
- Y. Gorlin and T. F. Jaramillo, *J. Am. Chem. Soc.*, 2010, **132**, 13612–13614.
- (a) E. R. Stobbe, B. A. de Boer and J. W. Geus, *Catal. Today*, 1999, **47**, 161–167; (b) R. Alizadeh, E. Jamshidi and G. Zhang, *J. Nat. Gas Chem.*, 2009, **18**, 124–130.
- (a) J. Shin, R. M. Anisur, M. K. Ko, G. H. Im, J. H. Lee and I. S. Lee, *Angew. Chem., Int. Ed.*, 2009, **48**, 321–324; (b) T.-L. Ha, H. J. Kim, J. Shin, G. H. Im, J. W. Lee, H. Heo, J. Yang, C. M. Kang, Y. S. Choe, J. H. Lee and I. S. Lee, *Chem. Commun.*, 2011, **47**, 9176–9178.
- S. Lei, K. Tang, Z. Fang and H. Zheng, *Cryst. Growth Des.*, 2006, **6**, 1757–1760.
- (a) Y. Li, H. Tan, X.-Y. Yang, B. Goris, J. Verbeeck, S. Bals, P. Colson, R. Cloots, G. Van Tendeloo and B.-L. Su, *Small*, 2011, **7**, 475–483; (b) P. Q. Zhang, Y. G. Zhan, B. X. Cai, C. C. Hao, J. Wang, C. X. Liu, Z. J. Meng, Z. L. Yin and Q. Y. Chen, *Nano Res.*, 2010, **3**, 235–243.
- T. Takashima, K. Hashimoto and R. Nakamura, *J. Am. Chem. Soc.*, 2011, **134**, 1519–1527.
- M. E. Bodini, L. A. Willis, T. L. Riechel and D. T. Sawyer, *Inorg. Chem.*, 1976, **15**, 1538–1543.
- (a) M. Matzapetakis, N. Karligiano, A. Bino, M. Dakanali, C. P. Raptopoulou, V. Tangoulis, A. Terzis, J. Giapintzakis and A. Salifoglou, *Inorg. Chem.*, 2000, **39**, 4044–4051; (b) F. Aguado, F. Rodriguez and P. Núñez, *Phys. Rev. B*, 2007, **76**, 094417.
- A. T. R. Williams, S. A. Winfield and J. N. Miller, *Analyst*, 1983, **108**, 1067–1071.
- (a) J. W. Lee, A. S. Hall, J.-D. Kim and T. E. Mallouk, *Chem. Mater.*, 2012, **24**, 1158–1164; (b) M. Salavati-Niasari, F. Davar and M. Mazaheri, *Polyhedron*, 2008, **27**, 3467–3471.
- F. Li, L. H. Zhang, D. G. Evans and X. Duan, *Colloids Surf., A*, 2004, **244**, 169–177.
- G. C. Silva, F. S. Almeida, A. M. Ferreira and V. S. T. Ciminelli, *J. Mater. Res.*, 2012, **15**, 403–408.
- F. Buciuman, F. Patcas, R. Craciun and D. R. T. Zahn, *Phys. Chem. Chem. Phys.*, 1999, **1**, 185–190.
- Y.-F. Han, F. Chen, Z. Zhong, K. Ramesh, L. Chen and E. Widjaja, *J. Phys. Chem. B*, 2006, **110**, 24450–24456.

- 24 (a) C.-C. Huang, N.-H. Khu and C.-S. Yeh, *Biomaterials*, 2010, **31**, 4073–4078; (b) H. Chen and J. He, *J. Phys. Chem. C*, 2008, **112**, 17540–17545.
- 25 (a) N. Kaneko, M. Kaneko and H. Takahashi, *Spectrochim. Acta, Part A*, 1984, **40**, 33–42; (b) V. Krishnakumar and S. Dheivamalar, *J. Raman Spectrosc.*, 2009, **40**, 627–631.
- 26 V. Ramakrishnan and J. M. T. Maroor, *Infrared Phys.*, 1988, **28**, 201–204.
- 27 (a) S. Kolesnik, B. Dabrowski and J. Mais, *J. Appl. Phys.*, 2004, **95**, 2582–2586; (b) K. R. Kittilstved and D. R. Gamelin, *J. Am. Chem. Soc.*, 2005, **127**, 5292–5293; (c) K. R. Kittilstved, D. A. Schwartz, A. C. Tuan, S. M. Heald, S. A. Chambers and D. R. Gamelin, *Phys. Rev. Lett.*, 2006, **97**, 037203.
- 28 B. N. Figgis and M. A. Hitchman, *Ligand Field Theory and Its Applications*, Wiley-VCH, New York, 2000.
- 29 C. R. Vestal and Z. J. Zhang, *J. Am. Chem. Soc.*, 2003, **125**, 9828–9833.
- 30 L. Zhang, J.-Q. Wang, J. Li, S. Zhang, Z. Jiang, J. Zhou, J. Cheng, T. Hu, W. Yan, X. Wei and Z. Wu, *Chem. Mater.*, 2012, **24**, 1676–1681.
- 31 S. Baruah, S. S. Sinha, B. Ghosh, S. K. Pal, A. K. Raychaudhuri and J. Dutta, *J. Appl. Phys.*, 2009, **105**, 074308.
- 32 S. S. Sinha, P. K. Verma, A. Makhil and S. K. Pal, *Rev. Sci. Instrum.*, 2009, **80**, 053109.
- 33 A. Kudo, K. Omori and H. Kato, *J. Am. Chem. Soc.*, 1999, **121**, 11459–11467.